Pergamon

Int. J. Heat Mass Transfer. Vol. 40, No. 11, pp. 2579–2593, 1997

Printed in Great Britain
0017-9310/97 $17.00+0.00

PII: S0017-9310(96)00297-9

Film boiling heat transfer of droplet streams and sprays

JOHN D. BERNARDIN and ISSAM MUDAWAR†

Boiling and Two-phase Flow Laboratory, School of Mechanical Engineering, Purdue University, West Lafayette, IN 47907, U.S.A.

(*Received* 2 *July* 1996 *and in final form* 16 *August* 1996)

Abstract—This paper presents an empirical approach to determining film boiling heat transfer of a spray from extrapolation of the heat transfer characteristics of an isolated droplet stream. First, an experimental investigation of film boiling heat transfer from a polished nickel surface to a continuous stream of monodispersed water droplets was performed for surface temperatures up to 400°C. Empirical correlations are presented for film boiling heat transfer rate and droplet heat transfer efficiency over a wide range of operating conditions. These single droplet stream correlations were then employed to predict film boiling heat transfer rates of both multiple droplet streams and sprays of uniform droplet size and velocity. By correctly accounting for differences in volumetric flux and droplet heat transfer efficiency, it is shown how the single droplet stream correlations facilitate the prediction of film boiling heat transfer of a dilute spray.

1. INTRODUCTION

Recent technological advancements and imposed environmental and economic constraints have resulted in greater demands for material with increased performance, better recyclability and lower cost. Several of these impositions have led to requirements for high heat dissipation rates and enhanced cooling control strategies such as in the processing or heat treating of metallic alloys. While pool boiling and jet impingement techniques have satisfactorily provided high heat dissipation rates, they have generally failed to insure uniform and controlled cooling because of large spatial variations in surface heat flux, especially for complex-shaped alloy parts. Spray cooling, on the other hand, has been found quite effective at satisfying both these requirements by dissipating enormous amounts of heat and possessing a high degree of adaptability and control for different part geometries. For example, recent studies have shown water sprays can be used to effectively control quench rate and material properties of heat treatable aluminum alloys [1, 2]. However, while spray quenching offers potential enhancement of material processing operations, its immediate integration is limited because of incomplete understanding of the complex fluid flow and heat transfer characteristics of sprays.

1.1. *Spray boiling curve*

To understand the fundamental heat transfer aspects of spray cooling, it is helpful to refer to the cooling curve or temperature-time history of a hot surface as it is quenched from a relatively high temperature. This curve, shown in Fig. 1, displays the temperature history for a surface (shown here for simplicity for the case of bath quenching) and exhibits the four distinct heat transfer regimes of film boiling, transition boiling, nucleate boiling, and single-phase liquid cooling. Each of these regimes possesses unique fluid flow and heat transfer characteristics. While the cooling rate in each regime is much greater with sprays than with bath quenching, the overall shape of the cooling curve is similar for both.

At extremely high surface temperatures, liquid–solid contact during spray quenching is very brief, as an insulating vapor layer quickly develops at the point of contact between the impinging droplets and the surface. Consequently, the heat transfer rate is relatively small, reflected by a slow decrease in the surface temperature. The film boiling regime persists to a lower temperature limit, known as the Leidenfrost point. Immediately below this limit exists the transition boiling regime in which the droplets begin to make more effective and prolonged contact with the solid surface resulting in higher heat transfer rates and a more rapid decrease in surface temperature. At the lower temperature boundary of the transition boiling regime, the critical heat flux point, the droplets begin to effectively wet and spread out across the surface. Below the critical heat flux temperature is the nucleate boiling regime where heat fluxes are quite large but decrease rapidly with decreasing surface temperature due to a sharp decrease in vapor bubble formation. Below the bubble incipience temperature, the lower boundary of the nucleate boiling regime, bubble nucleation ceases and heat transfer occurs by con-

† Author to whom correspondence should be addressed.

NOMENCLATURE

A_h	single droplet stream heater surface area [m^2]
a_1, a_2, a_3, a_4	empirical constants in equation (15)
B	dimensionless superheat parameter, $c_{p,g}\Delta T_{sat}/h_{fg}$
c_p	specific heat at constant pressure [J kg^{-1} K^{-1}]
D	droplet generator orifice diameter [m]
d_0	droplet diameter [m]
d_{32}	Sauter mean diameter [m]
f	frequency [s^{-1}]
h_{fg}	latent heat of vaporization [J kg^{-1}]
h'_{fg}	modified latent heat of vaporization, $c_{p,f}(T_{sat}-T_f)+h_{fg}$ [J kg^{-1}]
K	dimensionless vapor property parameter, $k_g/(c_{p,g}\mu_g)$
k	thermal conductivity [W m^{-1} K^{-1}]
N	number of droplet streams
n	empirical constant in equation (6)
Q	volumetric flow rate [m^3 s^{-1}], total amount of heat transfer [J]
Q_{sd}	total heat transfer to a single impinging droplet [J]
Q_{max}	maximum possible heat transfer to a single impinging droplet (J)
Q''_{sp}	spray volumetric flux [m^3 s^{-1} m^{-2}]
q	heat transfer rate [W]
q''	heat flux [W m^{-2}]
S	dimensionless thermal capacitance, $(k\rho c_p)_s^{0.5}/(k\rho c_p)_{steel}^{0.5}-1$
T	temperature [°C]
u_m	spray mean droplet velocity [m s^{-1}]
u_0	droplet velocity [m s^{-1}]
We	droplet Weber number, $\rho_f u_0^2 d_0/\sigma$
x, y	coordinates along spray impact area [m].

Greek symbols

ΔT_f	T_s-T_f [°C]
ΔT_{sat}	surface superheat, T_s-T_{sat} [°C]
ε	droplet heat transfer efficiency
λ	wavelength [m]
μ	dynamic viscosity [N s m^{-2}]
ρ	density [kg m^{-3}]
σ	surface tension [N m^{-1}].

Subscripts

f	liquid
fg	difference between liquid and vapor
g	vapor
meas	measured
opt	optimum
pred	predicted
s	solid, surface
sat	saturation
sd	single droplet
sp	spray
ss	single droplet stream.

duction through the liquid film created by the impinging droplets.

The heat transfer behavior described above is quite general and can be significantly altered through manipulation of the droplet hydrodynamic parameters such as diameter, velocity, frequency and volumetric flux, as well as surface roughness. This work concerns film boiling heat transfer of sprays and its dependence on these important parameters.

1.2. *Droplet heat transfer literature*

In previous studies by the authors [3, 4], qualitative assessments of the fluid flow and heat transfer characteristics of droplets impacting heated surfaces were made. Still and high speed photography was used to construct a photographic library and droplet regime maps which identified the effects of droplet velocity, surface temperature, and surface roughness on the spreading and heat transfer characteristics of impinging droplets. While these studies provided valuable insight into impinging droplet heat transfer, they did not constitute a direct means of predicting heat transfer rates of droplets or sprays.

Film boiling heat transfer rates associated with impinging droplets have typically been assessed experimentally by determining an average heat flux, heat transfer coefficient, or droplet heat transfer efficiency, the latter is defined as

$$\varepsilon = \frac{Q_{sd}}{Q_{max}} = \frac{Q_{sd}}{\rho_f \frac{\pi d_0^3}{6} h'_{fg}}. \quad (1)$$

Previous investigations have shown that for a given fluid, these parameters are influenced to varying degrees by droplet, velocity and frequency, as well as surface temperature.

Bolle and Moureau [5] and Takeuchi *et al.* [6] reported an increase in the film boiling heat transfer rate with increasing droplet diameter, which was speculated to result from increased liquid–solid contact area. Takeuchi *et al.* also reported the droplet heat transfer efficiency decreases with increasing droplet diameter.

Pedersen [7] and Takeuchi *et al.* [6] reported film boiling heat transfer rate increases with increasing

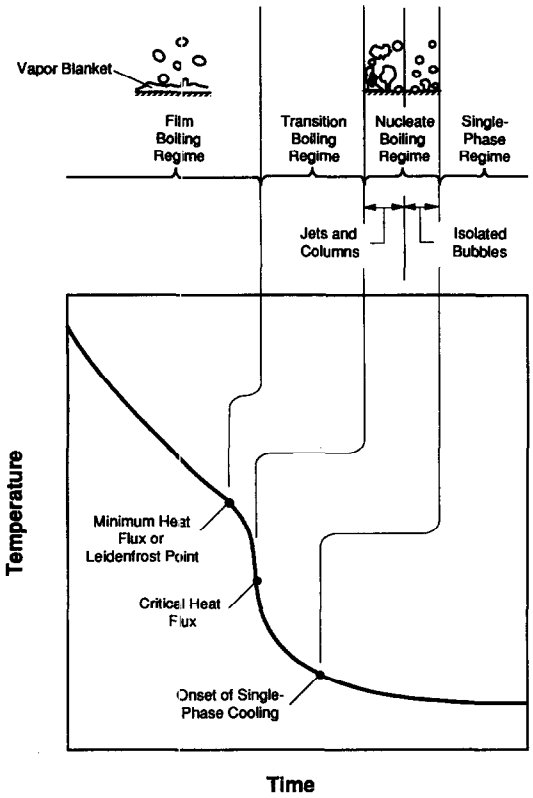

Fig. 1. Temperature–time history of a surface during quenching in a bath of liquid.

droplet velocity for relatively small water droplets ($0.20\times10^{-3}\leqslant d_0\leqslant 0.56\times10^{-3}$ m, $2.2\leqslant u_0\leqslant 10.1$ m s^{-1}). Bernardin *et al.* [3] reported a similar trend for larger and slower water droplets ($d_0=3.0\times10^{-3}$ m, $0.7\leqslant u_0\leqslant 2.34$ m s^{-1}). Contrary to these findings, Shi *et al.* [8] found that heat transfer rate for large water droplets ($2.0\times10^{-3}\leqslant d_0\leqslant 5.0\times10^{-3}$ m, $0.5\leqslant u_0\leqslant 3.0$ m s^{-1}) decreases with an increase in impact velocity. This trend was also predicted in analytical studies by Bolle and Moureau [5] and Inada and Yang [9]. In several studies, heat transfer efficiency was reported to increase with increasing droplet velocity [6, 7, 10].

Studies by Takeuchi *et al.* [6], Senda *et al.* [11], and Bernardin *et al.* [3] revealed film boiling heat transfer rate for water droplets ($0.3\times10^{-3}\leqslant d_0\leqslant 3.0\times10^{-3}$ m, $0.7\leqslant u_0\leqslant 7.0$ m s^{-1}) increases with increasing droplet frequency over a range of 0.67–1000 s^{-1}. In addition, Takeuchi *et al.* [6] and Senda *et al.* [11] reported heat transfer efficiency decreases with increasing frequency, speculating this was the result of interference of impinging droplets and residual liquid remaining on the surface from previous droplets.

The film boiling regime for impinging droplets is characterized by extremely short liquid–solid contact times on the order of 1–10 ms [3, 12] during which a thin vapor layer is rapidly established between the liquid and solid surface. Consequently, heat transfer efficiency and heat transfer rate in this regime are weak functions of surface temperature. Wachters and Westerling [13] and Bernardin *et al.* [3] performed film boiling heat transfer measurements of large water droplets ($d_0\approx 2.0\times10^{-3}$–$3.0\times10^{-3}$ m) impinging upon gold surfaces with surface temperature ranges of 250–370°C and 220–280°C, respectively, and found heat transfer rate is fairly insensitive to changes in surface temperature. In several studies, the film boiling heat transfer rate was observed to increase to varying degrees with increasing surface temperature [5, 6, 8, 11].

Pedersen [7], Takeuchi *et al.* [5] and Senda *et al.* [11] reported droplet heat transfer efficiency for water droplets ($0.2\times10^{-3}\leqslant d_0\leqslant 0.6\times10^{-3}$ m) remains relatively constant over surface temperatures ranging from 200 to 620°C, while for similar size droplets, Liu and Yao [10] reported modest increases in heat transfer efficiency with increasing surface temperature for $197\leqslant T_s\leqslant 974$°C.

1.3. *Single droplet heat transfer correlations*

The influence of fluid properties and geometrical parameters on droplet film boiling heat transfer rate have been investigated by use of analytical techniques [9, 14] or through extensive experimental investigation. The significant empirical correlations which are most relevant to the current study are presented below.

Bolle and Moureau [5] developed the following semi-empirical expression for the total heat transfer during initial contact between the impinging droplet and the heated surface prior to vapor production in the film boiling regime,

$$Q_{sd}=0.82(k\rho c_p)_s^{0.5}(T_s-T_f)\frac{d_0^{2.5}}{u_0^{0.5}}. \tag{2}$$

Takeuchi *et al.* [6] correlated both heat transfer rate and heat transfer efficiency with respect to droplet frequency, velocity, and diameter,

$$q_{ss}\propto f^{0.95}u_0^{0.65}d_0^{2.62} \tag{3}$$

$$\varepsilon_{ss}\propto f^{-0.05}u_0^{0.65}d_0^{-0.38} \tag{4}$$

for water droplets over the following ranges: $0.29\times10^{-3}\leqslant d_0\leqslant 0.56\times10^{-3}$ m, $2.2\leqslant u_0\leqslant 4.8$ m s^{-1}, $T_s\leqslant 600$°C and $10\leqslant f\leqslant 100$ s^{-1}.

More recently, Deb and Yao [15] used dimensional analysis to arrive at the following expression for heat transfer efficiency of impinging droplets in the transition and film boiling regimes based on the droplet Weber number ($We=\rho_f u_0^2 d_0/\sigma$), and dimensionless parameters related to wall superheat, $B=c_{p,g}(T_s-T_{sat})/h_{fg}$, vapor properties, $K=k_g/(c_{p,g}\mu_g)$, and thermal capacity of the solid wall, $S=(k\rho c_p)_s^{0.5}/(k\rho c_p)_{steel}^{0.5}-1$,

$$\varepsilon_{sd} = 0.02729 \exp\left(\frac{0.081\sqrt{\ln(We/35+1)}}{(B+S/60.5)^{1.5}}\right) + 0.21085KB\exp\left(\frac{-90}{We+1}\right) \quad (5)$$

where all liquid and vapor properties are evaluated at the saturation temperature.

1.4. *Spray heat transfer literature*

Previous investigations of the film boiling regime for sprays have generally been concerned with parametric trends of surface heat flux and corresponding heat transfer coefficients. Many of these studies employed full cone nozzles to produce water sprays with wide ranges of droplet size, droplet velocity, and spray volumetric flux [16–20], while others used an impulse technique to break up a liquid stream into a spray of droplets with uniform size and velocity [21, 22]. In most of these studies, spray volumetric flux (volume flow rate per unit area) was found to be the key parameter influencing film boiling heat flux,

$$q''_{sp} \propto Q''^{n}_{sp} \quad 0.26 \leqslant n \leqslant 1.0. \quad (6)$$

Unlike the other boiling regimes, heat flux in the film boiling regime was observed to be a weak function of both surface temperature [16, 17, 20] and liquid subcooling [17, 18]. In addition, heat flux was found to increase slightly with increasing droplet velocity and was nearly independent of droplet diameter [18, 20, 23]. Choi and Yao [21, 22] reported heat transfer rate increases with increasing droplet diameter and velocity for dilute sprays, but is insensitive to these same parameters for dense sprays because of droplet interference upon impact. Both studies showed that for dilute and dense sprays, direct droplet–surface contact is responsible for the majority of heat transfer while air convection and radiation accounts for less than 30%. While no quantitative categorization of dilute and dense sprays exists, Yao and Choi [22], Delcorio and Choi [24], Deb and Yao [15], and Klinzing *et al.* [20] have reported local liquid mass flux values ranging from 0.2 to 3.5 kg m^{-2} s^{-1} as the boundary between the two spray regimes.

Empirical film boiling heat transfer correlations for water sprays based on local spray hydrodynamic parameters of liquid volumetric flux, Q''_{sp}, mean droplet velocity, u_m, and Sauter mean drop diameter, d_{32}, were developed by Klinzing *et al.* [20] over a wide range of operating conditions ($Q''_{sp} = 0.58\times10^{-3} - 9.96\times10^{-3}$ m^3 s^{-1} m^{-2}, $u_m = 10.1-29.9$ m s^{-1}, $d_{32} = 0.137\times10^{-3} - 1.350\times10^{-3}$ m) and surface temperatures up to 520°C. Two distinct film boiling regimes were identified and spray heat flux was correlated with respect to low flux sprays ($Q''_{sp} < 3.5\times10^{-3}$ m^3 s^{-1} m^{-2}) and high flux sprays ($Q''_{sp} > 3.5\times10^{-3}$ m^3 s^{-1} m^{-2}) according to equations (7) and (8), respectively,

$$q''_{sp} = 63.250\Delta T_f^{1.691} Q''^{0.264}_{sp} d_{32}^{-0.062} \quad (7)$$

$$q''_{sp} = 1.413\times10^{5}\Delta T_f^{0.461} Q''^{0.566}_{sp} u_m^{0.639}. \quad (8)$$

Analytical modeling of spray film boiling by extrapolating empirical heat transfer relations of single droplets has lacked success. For example, Moriyama *et al.* [25] developed an analytical model for the local film boiling heat transfer coefficient for a spray based on an empirical heat transfer relation for a single impinging droplet ($We < 75$) corrected for the volumetric flux, the droplet diameter, and the droplet velocity distributions of the spray. Comparisons of the model predictions with experimental data showed errors ranging from a few to several hundred per cent, the weaknesses being related to the velocity limitation of the single droplet model and poor account of droplet interference within a spray. Deb and Yao [15] constructed an analytical heat transfer model for a spray with uniform droplet diameter and velocity by accounting for droplet contact heat transfer, bulk air convection and radiation. The droplet contact heat transfer was described by a semi-empirical heat transfer effectiveness correlation originally developed for single impinging droplets. For dilute sprays, the model exhibited fair agreement with experimental data well into the film boiling regime but with significant error near the Leidenfrost point. In a later study by Deb and Yao [26], a dense spray model was formulated as a combination of the asymptotic conditions of the earlier dilute spray model and a pool boiling model, the latter of which represents an extreme surface flooding condition of a dense spray. Delcorio and Choi [24] modeled the film boiling heat transfer rate in dilute and dense sprays by using a sub-model of the sensible heat exchange of single impinging droplets and properly accounting for spray droplet number density and reduction in liquid–solid contact area due to multiple droplet interference. The dilute spray model exhibited fair agreement with experimental data, however, the dense spray model showed a discrepancy of more than 100%.

1.5. *Modeling of sprays*

While many qualitative observations have been made concerning film boiling heat transfer of impinging droplets and sprays, accurate quantitative assessments have been incomplete. In addition, the fluid and heat transfer characteristics of droplets and sprays have generally been investigated independently. Consequently, a comprehensive spray film boiling model based upon single droplet stream characteristics is currently unavailable. The objective of the present study is to construct a spray film boiling heat transfer correlation based upon the heat transfer characteristics of a single droplet stream and the statistical droplet distributions of sprays. This is accomplished using the following approach:

(1) Quantitative assessments of the influence of droplet velocity, droplet diameter, and surface temperature on film boiling heat transfer rate are made for a single stream of impinging droplets.

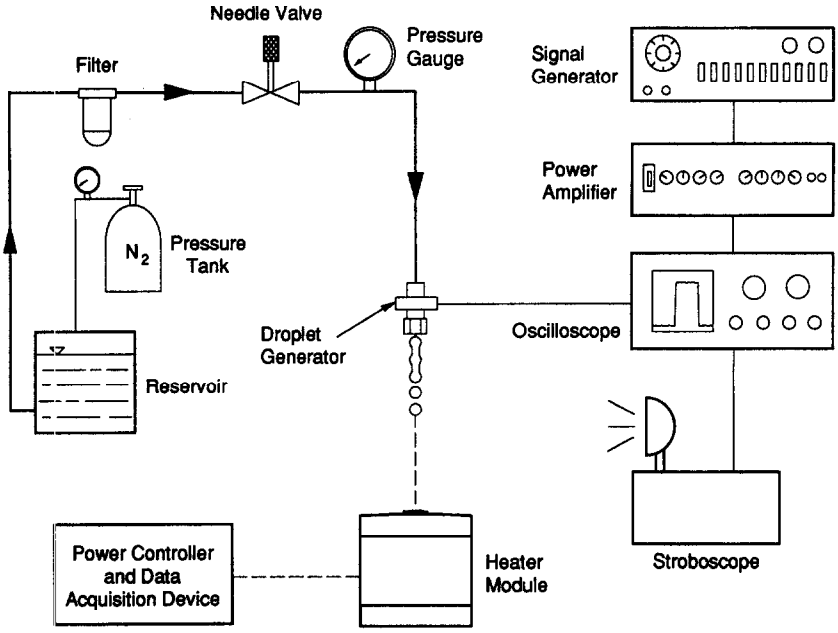

Fig. 2. Schematic diagram of the droplet heat transfer facility.

(2) Empirical correlations based on single droplet stream characteristics are used to predict film boiling heat transfer to arrays of droplet streams. The accuracy of this technique and limitations imposed by interference effects are carefully ascertained.

(3) Film boiling heat transfer rate of sprays is predicted using the single droplet stream correlations and the spray's volumetric flux. The accuracy of this technique and limitations imposed by droplet interference are also determined for sprays.

2. EXPERIMENTAL METHODS

2.1. *Droplet generator facility*

The apparatus shown in Fig. 2 was constructed to investigate boiling heat transfer from a heat source to both single and multiple streams of uniform droplets. The main components of this apparatus were a fluid delivery system, a droplet generator and associated electronic hardware, and a heater module.

The fluid delivery system consisted of a reservoir, a compressed nitrogen tank, stainless steel tubing, fittings, valves and a 5 μm filter. Deionized water was used exclusively as the working fluid.

The two droplet generators illustrated in Fig. 3(a) were used to produce single and multiple droplet streams. Except for differences in size, the droplet generators were similar in construction. Each was composed of a brass or stainless steel main body and cap, a piezo-ceramic crystal, a rubber gasket, and a stainless steel orifice plate. Attached to the main body were stainless steel fittings for the water inlet and air bleed lines. Four different steel orifice plates with orifice diameters of 0.130, 0.249, 0.343 and 0.533×10^{-3} m produced droplets with respective diameters of 0.244, 0.468, 0.645 and 1.002×10^{-3} m for the single droplet generator. Orifice plates having symmetric four and nine hole patterns, Fig. 3(b), with orifice diameters of either 0.130 or 0.249×10^{-3} m were used in conjunction with the multiple droplet generator to produce uniformly distributed heat transfer rates across the heater surface and minimize neighboring droplet stream interference. The four hole pattern was designed with equal heater surface areas on either side of a base circle passing through the impact centers of the four droplet streams. The nine hole pattern provided a staggered droplet stream configuration with equal distances between nearest orifice holes. The cap and gasket were used to attach the orifice plates to the generator and allow cleaning or changing of the plates.

Vibrating droplet generators have been used in a variety of studies [27–30] to produce a stream or spray of monodispersed droplets. For a typical generator, liquid is forced through a small orifice at a constant flow rate to develop a laminar jet. By using a vibrating device operating over a narrow frequency range, the jet is mechanically excited and caused to disintegrate into a periodic system of uniformly sized droplets. The principle of operation of the generator is based upon the instability of liquid jets as discussed by Lord Rayleigh [31]. He showed through a surface energy argument, that a liquid jet which is affected by only surface tension forces will become unstable for any axisymmetric disturbance whose wavelength is greater than the circumference of the jet. He also showed that the fastest-growing disturbance wavelength, λ_{opt}, is related to the jet diameter, D, by

$$\lambda_{opt} = 4.44D \tag{9}$$

and that disturbances of this wavelength lead to drop-

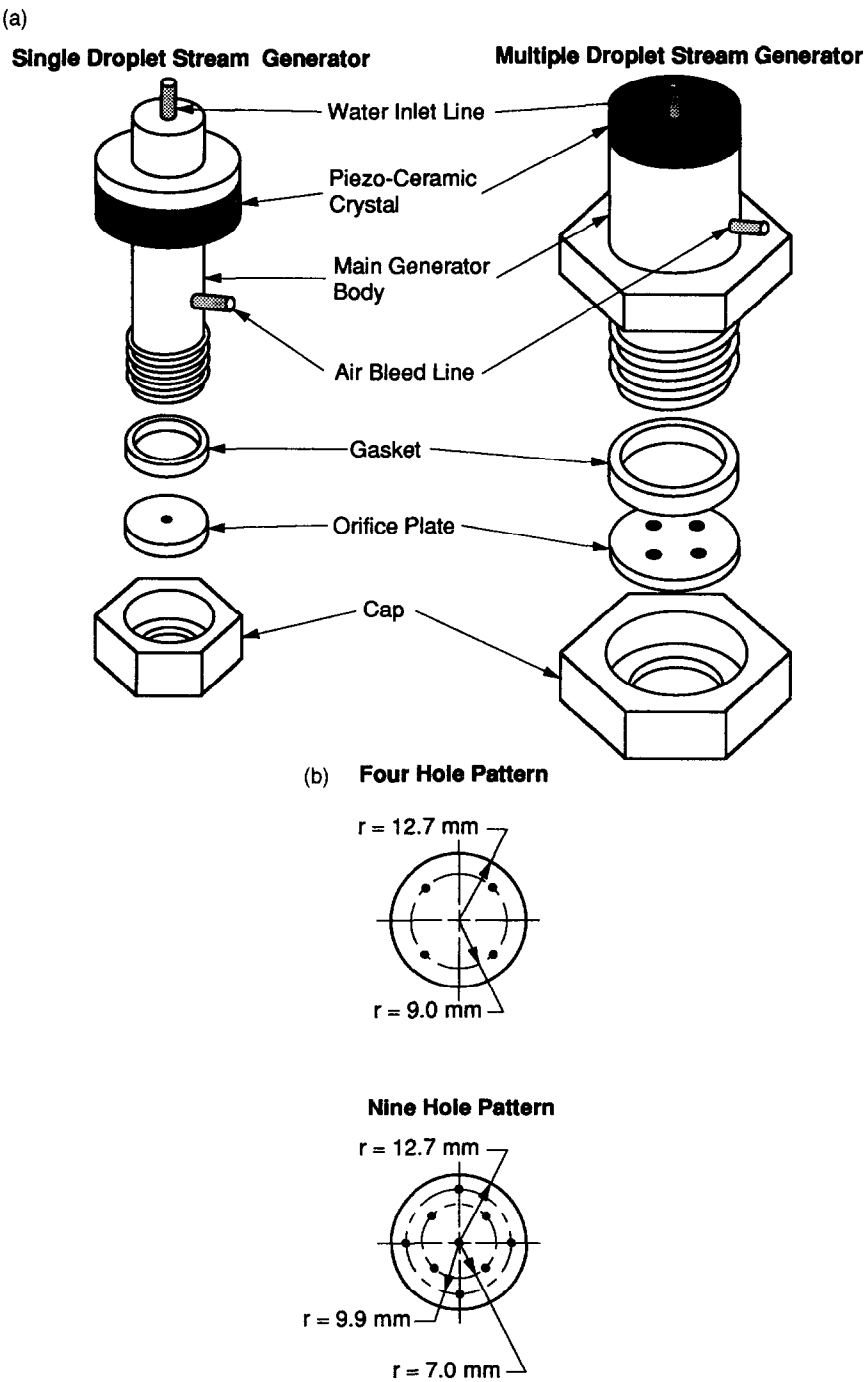

Fig. 3. Schematic diagrams of the (a) single and multiple droplet stream generators and (b) multiple droplet stream orifice plates.

lets whose diameter, d_0, is related to the orifice or jet diameter by

$$d_0 = 1.89D. \tag{10}$$

Schneider and Hendricks [32] determined experimentally that droplets could be produced by varying the disturbance wavelength over the following range

$$3.5D < \lambda < 7.0D. \tag{11}$$

Assuming the jet diameter does not contract when exiting the orifice, conservation of mass relates the droplet velocity, u_0, to the volumetric flow rate, Q, and jet diameter,

$$u_0 = \frac{4Q}{\pi D^2}. \tag{12}$$

The optimum jet breakup frequency can be related

to the droplet velocity and optimum disturbance wavelength or jet diameter by

$$f_{opt} = \frac{u_0}{\lambda_{opt}} = \frac{u_0}{4.44D}. \quad (13)$$

In this study, the droplet generator disturbances were supplied by an electrical signal generator connected to a power amplifier driving a piezo-ceramic crystal. An oscilloscope was used to accurately determine the operating frequency and a strobe light, connected to the signal generator, was used to verify the successful breakup of the liquid jets.

The heater modules illustrated in Figs. 4(a) and (b) were used, respectively, to measure heat transfer rates to single and multiple impinging droplet streams. For both modules, the heater body was made of oxygen free copper while the test surface was polished and nickel plated to a thickness of 0.025 mm (0.001 in) to minimize oxidation and corrosion. The instrumented portion of the heaters consisted of a calorimeter section with four type K thermocouples made from 0.076 mm (0.003 in) wires, spaced 2.54 mm (0.10 in) apart along the axis of each module. The thermocouple wires were inserted into the modules with 0.343 mm (0.135 in) diameter ceramic tubes. A finite element program was used to optimize the heater module design to ensure a one-dimensional heat flow pattern along the instrumented calorimeter section. Since the thermocouple holes accounted for a small percentage of the cross-sectional area of the calorimeter section, their effect on heat flux was assumed to be negligible. For the single droplet stream module, heat was supplied by a variable voltage transformer which was connected to a 120 V, 200 W electrical resistance heater wrapped around the lower, thicker portion of the module. The multiple droplet stream module used three 120 V, 150 W cartridge heaters in addition to the 120 V, 200 W wrap-around heater used with the single droplet stream module. A computer-driven data acquisition system was used to monitor temperature profiles in the heater modules. A one-dimensional temperature curve fit was extrapolated to determine the surface temperature and average surface heat flux. Figure 5(a) shows a typical experimental heat flux curve obtained from the single droplet stream heater module and Fig. 5(b) displays corresponding temperature profiles for several power inputs. These temperature profiles demonstrate the linearity of the temperature distribution and support the one-dimensional heat flow assumption. An error analysis based on the placement and calibration errors of the thermocouples yielded a maximum error of 6% in heat flux measurement.

The heater modules were mounted in a container fabricated from Nylon and G-7 and G-10 insulating plastic, as shown in Fig. 6 for the single droplet stream heater module. Insulating spacers made from a high temperature ceramic, were positioned between the container and heater module mounts. The remainder

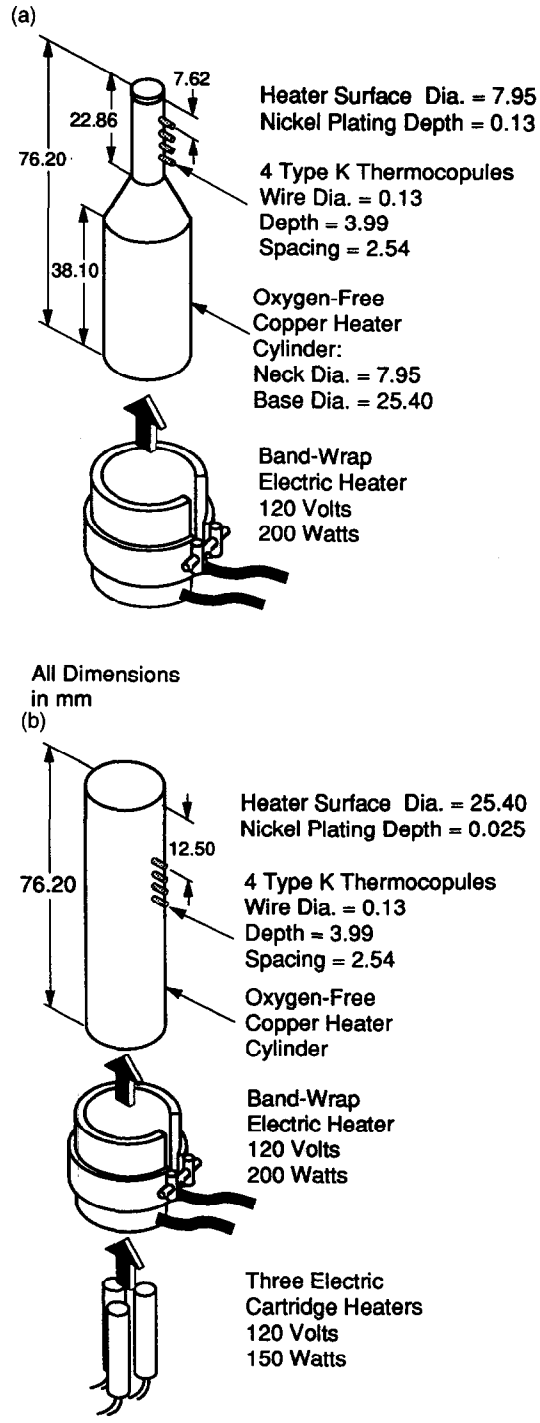

Fig. 4. Schematic diagrams of the (a) single droplet stream and (b) multiple droplet stream heater assemblies.

of the container was filled with perlite, a crushed stone which effectively insulated the heater module. Stainless steel fittings on the side of the container served as feed-throughs for thermocouple and electrical wires. This module design was capable of surface temperatures in excess of 500°C and steady-state heat fluxes up to 3.63×10^6 W m^{-2} for the single droplet stream heater module.

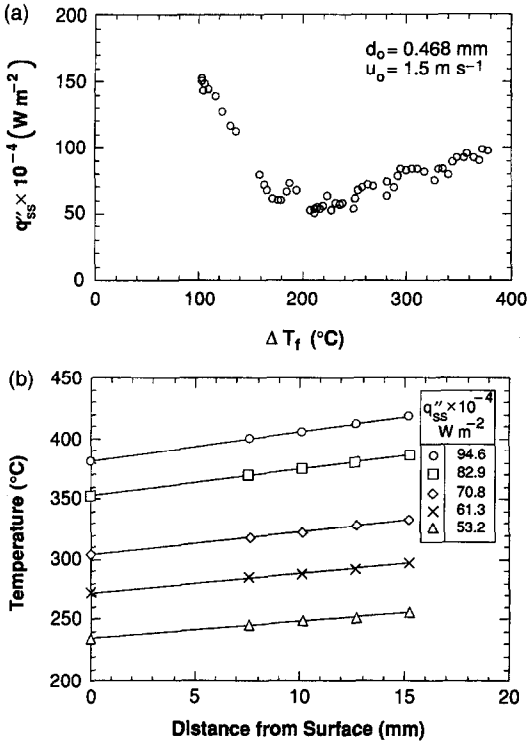

Fig. 5. (a) Heat flux data from the single droplet stream heater and (b) corresponding calorimeter temperature profiles.

The heat transfer measurements commenced by setting the liquid volumetric flow rate from the droplet generator to correspond to the desired droplet velocity for the given orifice diameter. The volumetric flow rate was measured using a graduated cylinder and a stop watch, and adjusted by a needle valve. Next, the piezo-ceramic crystal on the droplet generator was activated by setting the optimum liquid jet breakup frequency for the given flow conditions on the signal generator. A stroboscope was used to fine tune the droplet generator to obtain optimum breakup of the liquid stream into discrete, coherent droplets.

Once the desired droplet frequency was obtained, the heater module was allowed to heat up to about 425°C, after which it was positioned beneath the impinging droplet stream. A computer-driven data acquisition system was used to retrieve the calorimeter temperature profile as the power was slowly decremented to obtain quasi-steady film boiling heat flux and surface temperature data. Upon reaching the Leidenfrost point, the heater module was removed from the droplet stream and allowed to heat back up to 425°C, after which the measurements were repeated to insure reproducibility. This entire procedure was performed for four different droplet diameters and a range of droplet velocities for the single droplet stream as detailed in Table 1. For the multiple droplet stream study, the same procedure was used with four and nine droplet stream configurations and various droplet diameters and velocities.

2.2. *Spray facility*

A schematic diagram of the spray test facility is shown in Fig. 7. Complete details of this facility can

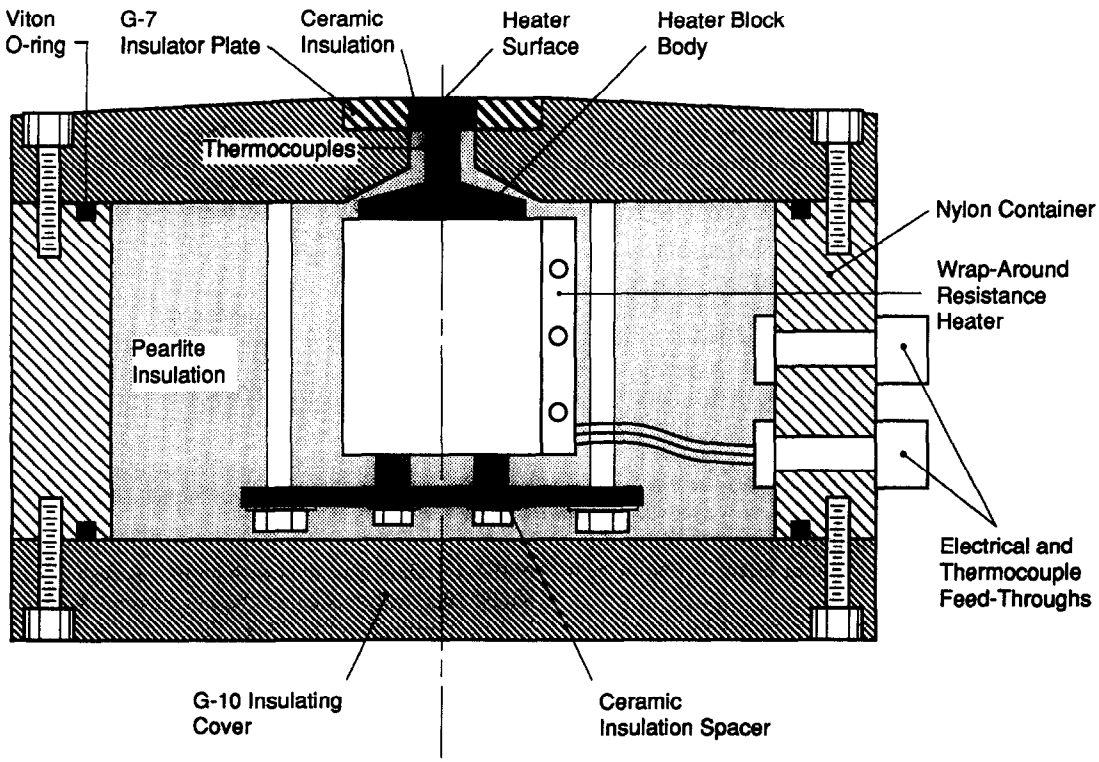

Fig. 6. Schematic diagram of the single droplet stream heater within the insulating container.

Table 1. Single droplet stream data matrix

Test number	$d_0 \times 10^3$ [m]	$Q_{ss} \times 10^9$ [$m^3 s^{-1}$]	u_0 [$m s^{-1}$]	f [s^{-1}]
1	0.250	49	3.7	6454
2	0.250	49	3.7	6454
3	0.250	48	3.6	6296
4	0.250	48	3.6	6296
5	0.250	63	4.8	8311
6	0.250	63	4.8	8311
7	0.250	40	3.0	5218
8	0.250	40	3.0	5218
9	0.250	78	5.8	10 162
10	0.250	78	5.8	10 162
11	0.250	94	7.1	12 327
12	0.250	94	7.1	12 327
13	0.468	100	2.1	1867
14	0.468	100	2.1	1867
15	0.468	97	2.0	1817
16	0.468	97	2.0	1817
17	0.468	74	1.5	1372
18	0.468	74	1.5	1372
19	0.468	120	2.5	2233
20	0.468	120	2.5	2233
21	0.645	144	1.6	1032
22	0.645	144	1.6	1032
23	0.645	177	1.9	1265
24	0.645	177	1.9	1265
25	0.645	177	1.9	1265
26	0.645	201	2.2	1436
27	0.645	201	2.2	1436
28	0.645	201	2.2	1436
29	1.002	253	1.1	481
30	1.002	253	1.1	481
31	1.002	253	1.1	481
32	1.002	227	1.0	432
33	1.002	227	1.0	432
34	1.002	277	1.2	527
35	1.002	277	1.2	527
36	1.002	277	1.2	527
37	1.002	277	1.2	527

be found in Mudawar and Valentine [33], so only a brief description is given here. The spray chamber consisted of a 114 l (30 gallon) reservoir and a three-dimensional translator for the spray nozzle. Water from the reservoir was pumped to the spray nozzle by a stainless steel vain pump capable of delivering up to 2.80×10^{-4} $m^3 s^{-1}$ (4.45 gpm) at 689.5 kPa (100 psig). Two rotameters and a stainless steel pressure gage were used to monitor the spray flow rate and spray nozzle upstream pressure, respectively. The insulated heater module container, power supply and data acquisition system described previously for the droplet generator facility were also employed with the spray facility to measure spray film boiling heat transfer rates.

A fan spray nozzle of type A described by Hall [34], operating at 138 kPa (20 psig), provided a dilute spray at a downstream nozzle distance of 0.305 m (12 in) with a Sauter mean diameter of 0.463×10^{-3} m, a mean droplet velocity of 9.6 m s^{-1}, and a spray flux distribution given by

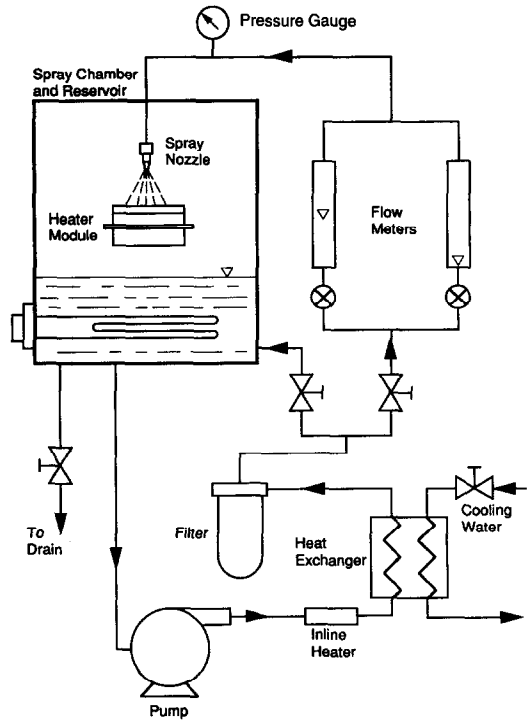

Fig. 7. Schematic diagram of the flow loop for the spray facility.

$$Q''_{sp}(x, y) = 2.63 \times 10^{-3} \exp(-163x^2 - 1130y^2) \quad (14)$$

where x and y are measured in m and correspond to the major and minor axes of the elliptical-shaped spray pattern. Spray heat transfer data was acquired at the following locations: (0, 0.0381), (0, 0.0254), (0, 0.0191) and (0, 0), corresponding to spray fluxes of 0.51×10^{-3}, 1.27×10^{-3}, 1.74×10^{-3} and 2.63×10^{-3} $m^3 s^{-1} m^2$.

The experimental procedure for the single spray facility was nearly identical to that described for the droplet generator facility. First, power was supplied to the heater module to raise its temperature to about 425°C. During this time, the nozzle was set to the desired location and the spray allowed to fully develop at the specified operating pressure. A flow diverter located beneath the spray nozzle prevented the liquid from striking the heated surface. Upon reaching initial operating conditions, the flow diverter was removed and the spray allowed to impinge upon the surface. The power to the heater module was slowly decreased to allow quasi-steady film boiling data to be recorded by the data acquisition system.

3. EXPERIMENTAL RESULTS

The results are presented in three subsections beginning with empirical correlations which described the heat transfer characteristics of a single droplet stream. Next, predictions based on the single stream correlations are compared to experimental heat transfer

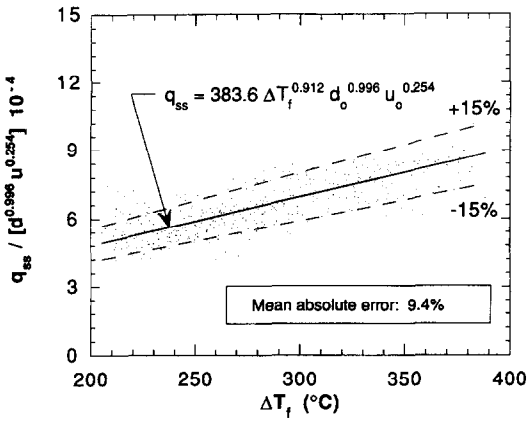

Fig. 8. Correlation of the single droplet stream film boiling heat transfer rate data.

rates of multiple droplet streams as a prelude to the final subsection concerning the determination of film boiling heat transfer for sprays.

3.1. *Single droplet stream correlations*

From the measured temperature profile data, the film boiling heat rate for a single stream was correlated according to the following equation:

$$q_{ss} = a_1 \Delta T_f^{a2} d_0^{a3} u_0^{a4}. \quad (15)$$

The surface temperature was found to have the greatest influence on heat transfer rate, thus its influence was weighted the highest among the experimental variables. The ΔT_f exponent was determined by averaging exponents for all of the q_{ss} vs ΔT_f data which resulted in a value of 0.912. Once this exponent was determined, the following correlation was obtained using a linear least squares fit to the data,

$$q_{ss} = 383.6 \Delta T_f^{0.912} d_0^{0.996} u_0^{0.254} \quad (16)$$

where q_{ss}, ΔT_f, d_0 and u_0 have the units of W, °C, m and m s^{-1}, respectively. Figure 8 shows the single stream data correlated according to equation (16) with a mean absolute error of 9.4%.

Two parameters, heat transfer rate discussed above, and the heat transfer efficiency, defined in equation (1), are commonly used to characterize droplet heat transfer. To determine droplet heat transfer efficiency, the maximum possible and actual amounts of heat transferred from the surface to a single droplet are needed. Expressions for these parameters are as follows:

$$Q_{max} = \rho_f \frac{\pi d_0^3}{6} h'_{fg} \quad (17)$$

$$Q_{sd} = \frac{q_{ss}}{f} = 899.8 \Delta T_f^{0.912} d_0^{1.996} u_0^{-0.746} \quad (18)$$

where the droplet frequency was determined by combining equations (10) and (13).

Substituting equations (17) and (18) into equation (1) gives the following expression for the film boiling heat transfer efficiency of each droplet in the single droplet stream,

$$\varepsilon_{ss} = \frac{1.719 \times 10^3}{\rho_f h'_{fg}} \Delta T_f^{0.912} d_0^{-1.004} u_0^{-0.746}. \quad (19)$$

Figure 9 shows ε_{ss} values for different surface temperatures, droplet velocities, and droplet diameters. Due to droplet interference, the heat transfer efficiencies predicted by equation (19) are lower than those predicted by equation (5) for non-interfering droplets. It is important to note equation (19) predicts that ε_{ss} decreases with increasing droplet velocity, which is opposite to the trend reported in [6]. A key difference between the two studies is the much lower frequency range in [6], 10–100 s^{-1}, i.e. negligible interference between droplets, compared to the present study, which included frequencies up to 12 327 s^{-1}.

The parametric ranges of validity for equations (16) and (19) are: $T_s = 200$–400°C, $T_f = 22$°C, $d_0 = 0.250 \times 10^{-3} - 1.002 \times 10^{-3}$ m and $u_0 = 1.0 - 7.1$ m s^{-1}. It must be emphasized these equations are only applicable to a droplet stream created with a generator which satisfies equations (9)–(13) since the droplet diameter, velocity, and frequency are all interrelated.

3.2. *Multiple droplet stream modeling*

Table 2 shows a comparison between the experimental film boiling heat transfer rate of N droplet streams, q_N, and the rate, Nq_{ss}, calculated by multiplying the single droplet stream heat transfer rate, equation (16), by the number of droplet streams. The uniform multiple droplet stream conditions were used as an intermediate step to investigate the feasibility of using single droplet stream characteristics to predict heat transfer rates in sprays. The low percentage difference between the data and predictions based on the single droplet stream correlation for most of the experimental conditions support the overall feasibility of this calculation method. Significant disagreement occurred with the nine stream configuration for the smallest droplet diameter. In this case, droplets from incoming streams bounced along the surface and coalesced into liquid globules which interfered with neighboring streams, greatly reducing the influence of droplet impact velocity and the heat transfer rate. This effect was not observed with the four stream configuration for either of the droplet diameters tested since interference between streams was non-existent. For the nine droplet stream configuration of the larger droplet diameter, an isolated liquid globule was anchored beneath each droplet stream, which helped reduce the effect of interference from liquid globules of neighboring streams.

3.3. *Spray modeling*

A semi-empirical model of film boiling heat flux for a spray, q''_{sp}, is constructed from the heat transfer rate correlation for a single droplet stream, q_{ss}. A spray may be idealized as N droplet streams impinging upon

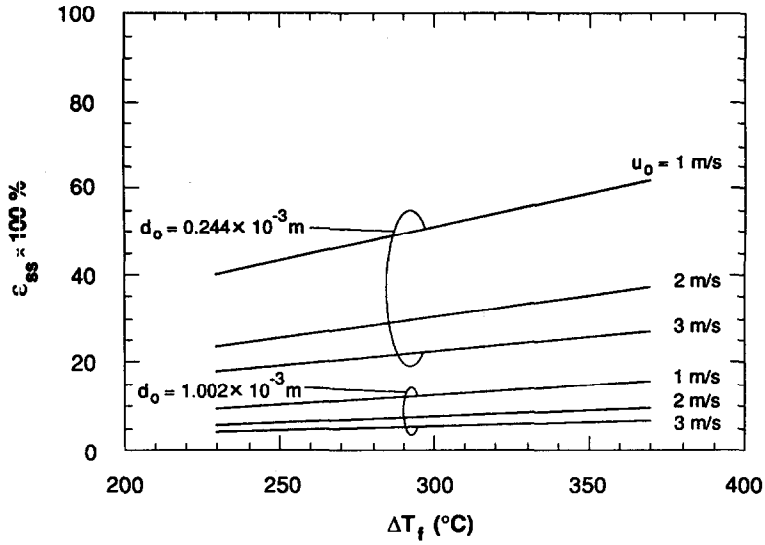

Fig. 9. Film boiling heat transfer efficiency of each droplet in a single droplet stream for different surface temperatures, droplet velocities and droplet diameters.

Table 2. Comparison of multiple droplet stream film boiling heat transfer data to predictions based on the single stream correlation

$d_0 \times 10^3$ [m]	u_0 [m s^{-1}]	ΔT_f [°C]	N	$q_{ss} \times N$ [W]	q_N [W]	Percentage difference
0.250	3.5	220	4	74.4	73.0	1.9
0.250	3.5	260	4	86.8	82.6	5.1
0.250	3.5	300	4	98.8	92.2	7.2
0.250	5.0	220	4	81.6	73.0	11.8
0.250	5.0	260	4	95.2	80.6	18.1
0.250	5.0	300	4	108.4	88.7	22.2
0.250	3.5	220	9	167.4	93.7	78.7†
0.250	3.5	260	9	195.3	97.8	99.7†
0.250	3.5	300	9	222.3	101.8	118†
0.250	5.0	220	9	183.6	109.4	67.8†
0.250	5.0	260	9	214.2	130.2	64.5†
0.250	5.0	300	9	243.9	150.5	62.1†
0.468	2.0	220	4	123.6	128.7	4.0
0.468	2.0	260	4	144.0	132.8	8.4
0.468	2.0	300	4	164.0	138.3	18.6
0.468	2.0	220	9	271.8	260.4	4.4
0.468	2.0	260	9	316.8	288.3	9.9
0.468	2.0	300	9	271.8	316.2	14.0

†Excessive interference of liquid from neighboring droplet streams reduced the heat transfer efficiencies of multiple streams in these runs leading to significant errors in calculations based on the single stream correlation.

a heater of area A_h. Figures 10(a) and (b) show photos of a single stream and a spray, respectively, and demonstrate that the multiple stream description of a spray is somewhat simplistic. The complex nature of droplet interactions and lack of uniformity of droplet formation in a spray warrant correcting the multiple droplet stream model by a ratio accounting for differences between the efficiency of a droplet stream and that of a spray. That is

$$q''_{sp} = q_{ss} \frac{N}{A_h} \frac{\varepsilon_{sp}}{\varepsilon_{ss}}. \tag{20}$$

The volumetric flux of a spray, when modeled as N droplet streams, can be written as

$$Q''_{sp} = \frac{\pi d_0^3}{6} f \frac{N}{A_h}. \tag{21}$$

Substituting equation (21) into equation (20) gives

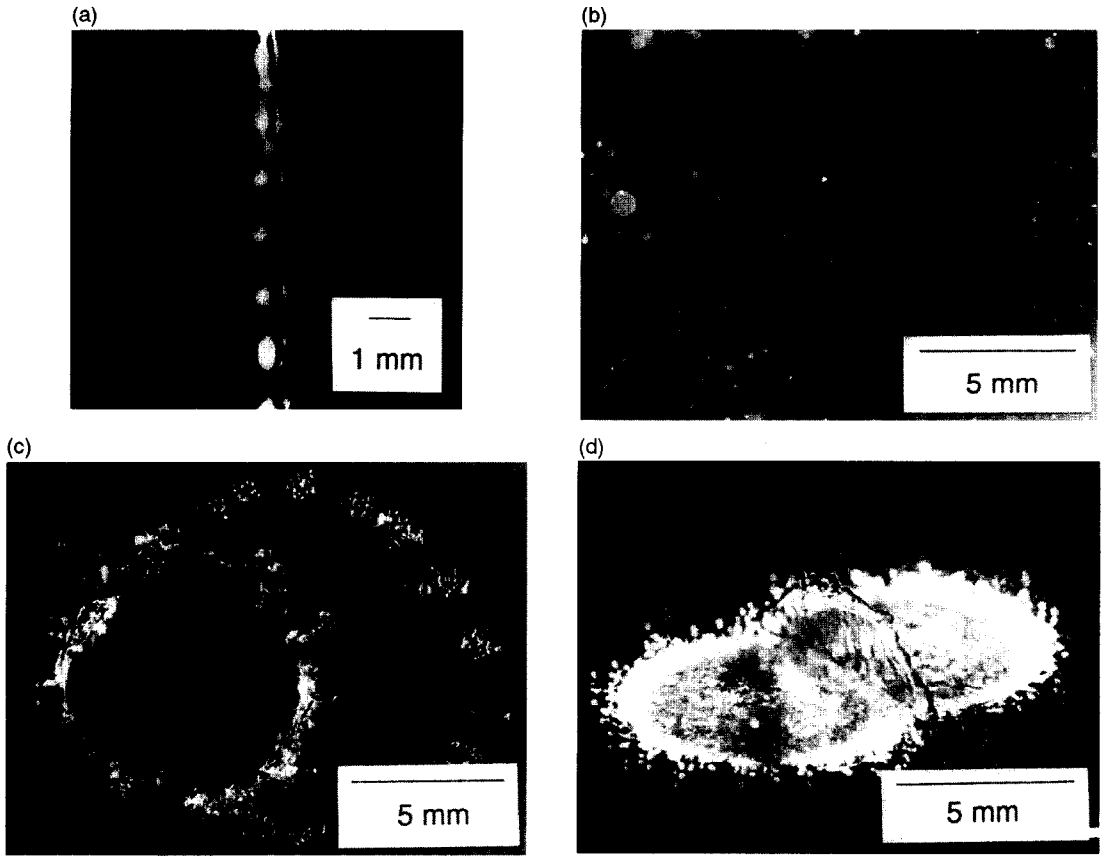

Fig. 10. Photographs of (a) single droplet stream with $d_0 = 0.645 \times 10^{-3}$ m, (b) center slice of spray from a fan nozzle operating at 138 kPa (20 psig), (c) successive droplet interference and (d) spreading droplet interference.

$$q''_{sp} = q_{ss} \frac{6Q''_{sp}}{\pi d_0^3 f} \frac{\varepsilon_{sp}}{\varepsilon_{ss}}. \quad (22)$$

The differences in the efficiency of a single stream from that of a spray are the result of two observed types of droplet interference. This interference can be successive, Fig. 10(c), where a droplet impinges on top of another spreading droplet, or as spreading, Fig. 10(d), in which neighboring droplet films collide. In each case, the effective liquid–solid contact area and corresponding heat transfer rate are reduced. For a conventional spray, the local droplet heat transfer efficiency is highly dependent upon the local volumetric spray flux, Q''_{sp}, a parameter frequently used to categorize spray density. For example, a 'dense' spray region would possess a relatively lower heat transfer efficiency than a 'dilute' spray region as a result of greater droplet interference in the former. Consequently, in modeling a spray from single droplet stream characteristics, a modification must be made to the single droplet stream heat transfer rate correlation to account for differences in heat transfer efficiency. The value of the droplet heat transfer efficiency for a spray, ε_{sp}, should fall between that of non-interfering single droplets, ε_{sd}, and that of a heavily interfering single droplet stream, ε_{ss}, equation (19). This relationship can be described using a linear interpolation based upon the local spray flux, Q''_{sp}, and a spray flux corresponding to a dense spray, $Q''_{sp,dense}$,

$$\varepsilon_{sp} = \varepsilon_{sd} - \frac{Q''_{sp}}{Q''_{sp,dense}}(\varepsilon_{sd} - \varepsilon_{ss}) \quad Q''_{sp} < Q''_{sp,dense} \quad (23a)$$

and

$$\varepsilon_{sp} = \varepsilon_{ss} \quad Q''_{sp} \geqslant Q''_{sp,dense}. \quad (23b)$$

The spray nozzle used in this study was identical to one used by Klinzing *et al.* [20], who found for that particular nozzle, a spray flux of $2\text{–}5 \times 10^{-3}$ m^3 s^{-1} m^{-2} corresponded to a transition region between dilute and dense sprays. Consequently, a value of 5×10^{-3} m^3 s^{-1} m^{-2} was chosen for $Q''_{sp,dense}$ to correspond to the boundary value for a fully dense spray.

The single droplet heat transfer efficiency expression given by Deb and Yao [15], equation (5), cannot be used in the present model. Over the experimental surface temperature range used in the present investigation, Deb and Yao's correlation predicts the droplet heat transfer efficiency decreases with increasing surface temperature, contrary to the present findings as well as those reported in the literature. Thus, in order to obtain a relation for ε_{sd}, the film boiling

heat flux correlation for low spray fluxes of Klinzing *et al.* [20], equation (7), was employed. Dividing equation (7) by the maximum possible heat flux, $\rho_f h'_{fg} Q''_{sp}$, gives the following spray film boiling heat transfer efficiency

$$\varepsilon_{sp} = \frac{63.25}{\rho_f h'_{fg}} \Delta T_f^{1.691} (Q''_{sp})^{-0.736} d_{32}^{-0.062}. \quad (24)$$

Extrapolating equation (24) down to an extremely low spray flux of 0.175×10^{-3} m^3 s^{-1} m^{-2}, corresponding to a spray so dilute that droplets do not interfere, as suggested from [20], the following expression is obtained for the single droplet heat transfer efficiency

$$\varepsilon_{sd} = \frac{3.68 \times 10^4}{\rho_f h'_{fg}} \Delta T_f^{1.691} d_{32}^{-0.062}. \quad (25)$$

It is important to note that the low flux value used in deriving equation (25) is simply an empirical limit which gave the smallest error in predicting spray heat flux data as discussed below.

Dividing equation (23a) by the single droplet stream heat transfer efficiency, ε_{ss}, gives

$$\frac{\varepsilon_{sp}}{\varepsilon_{ss}} = \frac{\varepsilon_{sd}}{\varepsilon_{ss}} \left(1 - \frac{Q''_{sp}}{Q''_{sp,dense}}\right) + \frac{Q''_{sp}}{Q''_{sp,dense}} \quad (26)$$

where ε_{ss} is defined as

$$\varepsilon_{ss} = \frac{\dfrac{q_{ss}}{f}}{\rho_f \dfrac{\pi d_0^3}{6} h'_{fg}}. \quad (27)$$

Substituting equations (26) and (27) into equation (22) and rearranging terms gives the following expression for the spray heat flux,

$$q''_{sp,pred} = q_{ss} \frac{6Q''_{sp}}{\pi d_0^3 f} \times \left\{ \frac{\pi d_0^3 f \rho_f h'_{fg} \varepsilon_{sd}}{6 q_{ss}} \left(1 - \frac{Q''_{sp}}{Q''_{sp,dense}}\right) + \frac{Q''_{sp}}{Q''_{sp,dense}} \right\}. \quad (28)$$

Equation (28) was developed for a local region of a spray across which the droplet diameter and velocity are constant. Replacing the single stream droplet diameter, d_0, and droplet velocity, u_0, with, respectively, the spray Sauter mean diameter, d_{32}, and the spray mean droplet velocity, u_m, and substituting for q_{ss}, equation (16), and f, equations (10) and (13), reduces equation (28) to the following

$$q''_{sp,pred} = \rho_f h'_{fg} Q''_{sp} \varepsilon_{sd} \left(1 - \frac{Q''_{sp}}{Q''_{sp,dense}}\right) + 1720 \Delta T_f^{0.912} d_{32}^{-1.004} u_m^{-0.746} \frac{(Q''_{sp})^2}{Q''_{sp,dense}}. \quad (29)$$

Thus, through knowledge of the single droplet heat transfer efficiency, equation (25), the spray parameters (d_{32}, u_m, Q''_{sp}), and the excess temperature of the surface, ΔT_f, equation (29) can be used to calculate the local spray film boiling heat flux. It must be emphasized that this correlation was established from empirical single droplet stream heat transfer data. Consequently, the model's greatest predictive capability corresponds to conditions which lie within the following parametric ranges used to establish the single droplet stream heat transfer correlation: $\Delta T_s = 180-380$°C, $d_{32} = 0.250 \times 10^{-3} - 1.002 \times 10^{-3}$ m and $u_m = 1.0-7.1$ m s^{-1}.

Table 3 compares spray film boiling heat fluxes predicted by equation (29) for water droplets with spray heat flux data, $q''_{sp,meas}$, obtained with the single spray facility and the heater module shown in Fig. 4(a) for three volumetric fluxes and three surface temperatures. A droplet diameter and a velocity of 0.463×10^{-3} m and 9.6 m s^{-1}, respectively, which are equal to the droplet Sauter mean diameter and mean droplet velocity of the spray, were used in the model calculations. The small percentage difference between the model predictions and experimental data,

$$\left| \frac{q''_{sp,meas} - q''_{sp,pred}}{q''_{sp,meas}} \right| \times 100\% \quad (30)$$

indicates good agreement for all cases with errors ranging from 2.2 to 23.3%. This close agreement is

Table 3. Comparison of spray heat flux model predictions and experimental results for water sprays with $d_{32} = 0.463 \times 10^{-3}$ m and $u_m = 9.6$ m s^{-1}

ΔT_f [°C]	q_{ss} [W]	$Q''_{sp} \times 10^3$ [m^3 s^{-1} m^{-2}]	$q''_{sp,pred} \times 10^{-5}$ [W m^{-2}]	$q''_{sp,meas} \times 10^{-5}$ [W m^{-2}]	Percentage difference
220	44.5	1.27	5.5	6.7	18.8
260	51.8	1.27	7.2	8.0	10.0
300	59.0	1.27	9.1	9.3	2.2
220	44.5	1.74	6.7	8.4	19.8
260	51.8	1.74	8.8	9.5	7.4
300	59.0	1.74	11.1	10.5	5.7
220	44.5	2.63	8.1	7.8	3.8
260	51.8	2.63	10.5	9.3	12.9
300	59.0	2.63	13.2	10.7	23.3

quite promising considering the obvious differences in droplet dynamics between a single droplet stream and a spray.

4. CONCLUSIONS

An experimental study was performed to investigate the film boiling heat transfer characteristics of a single stream of uniform water droplets and to employ these findings in modeling film boiling heat transfer of multiple droplet streams and dilute sprays. The key findings from this study are as follows:

(1) Empirical correlations were developed for the film boiling heat transfer rate and heat transfer efficiency for a single stream of water droplets. Key influential parameters in these correlations are surface temperature, droplet diameter and droplet velocity.

(2) The single droplet stream correlations were successfully extrapolated, without modification, to predict film boiling behavior of multiple droplet streams where interference between streams was insignificant.

(3) By accounting for the differences between a spray and an isolated droplet stream caused by droplet interference, the correlation for a single droplet stream heat transfer rate was successfully extrapolated to predict the film boiling heat flux for dilute sprays.

REFERENCES

1. J. D. Bernardin and I. Mudawar, Validation of the quench factor technique in predicting hardness in heat treatable aluminum alloys, *Int. J. Heat Mass Transfer* **38,** 863–873 (1995).
2. D. D. Hall and I. Mudawar, Predicting the impact of quenching on mechanical properties of complex-shaped aluminum alloy parts, *ASME J. Heat Transfer* **117,** 479–488 (1995).
3. J. D. Bernardin, C. J. Stebbins and I. Mudawar, Mapping of impact and heat transfer regimes of water drops impinging on a polished surface, *Int. J. Heat Mass Transfer* **40,** 247–267 (1997).
4. J. D. Bernardin, C. J. Stebbins and I. Mudawar, Effects of surface roughness on water droplet impact history and heat transfer regimes, *Int. J. Heat Mass Transfer* **40,** 73–88 (1997).
5. L. Bolle and J. C. Moureau, Spray cooling of hot surfaces. In *Multiphase Science and Technology* (Edited by G. F. Hewitt, J. M. Delhaye and N. Zuber), pp. 1–92. Hemisphere, New York (1982).
6. K. Takeuchi, J. Senda and K. Yamada, Heat transfer characteristics and the breakup behavior of small droplets impinging upon a hot surface, *Proceedings ASME/JSME Thermal Engineering Joint Conference* (Edited by Y. Mori and W. J. Yang), Honolulu, Hawaii, Vol. 1, pp. 165–172 (1983).
7. C. O. Pedersen, An experimental study of the dynamic behavior and heat transfer characteristics of water droplets impinging upon a heated surface, *Int. J. Heat Mass Transfer* **31,** 369–381 (1970).
8. M. H. Shi, T. C. Bai and J. Yu, Dynamic behavior and heat transfer of a liquid droplet impinging on a solid surface, *Exp. Thermal Fluid Sci.* **6,** 202–207 (1993).
9. S. Inada and W. J. Yang, Film boiling heat transfer for saturated drops impinging on a heating surface, *Int. J. Heat Mass Transfer* **37,** 2588–2591 (1994).
10. L. Liu and S. C. Yao, Heat transfer analysis of droplet flow impinging on a hot surface, *Proc. Seventh Int. Heat Transfer Conf.* (Edited by U. Grigull, E. Hahne, K. Stephan and J. Straub), Munich, Germany, Vol. 4, pp. 161–166 (1982).
11. J. Senda, K. Yamada, H. Fujimoto and H. Miki, The heat-transfer characteristics of a small droplet impinging upon a hot surface, *JSME Int. J.* **31,** 105–111 (1988).
12. M. A. Styricovich, Y. V. Baryshev, G. V. Tsiklauri and M. E. Grigorieva, The mechanism of heat and mass transfer between a water drop and a heated surface, *Proc. Sixth Int. Heat Transfer Conf.*, Toronto, Canada, Vol. 1, pp. 239–243 (1978).
13. L. H. Wachters and N. A. J. Westerling, The heat transfer from a hot wall to impinging water drops in the spheroidal state, *Chem. Engng Sci.* **21,** 1047–1056 (1966).
14. M. Cumo, G. E. Farello and G. Ferrari, Notes on droplet heat transfer, *Chem. Engng Prog. Symp. Series* **65,** 175–187 (1969).
15. S. Deb and S. C. Yao, Heat transfer analysis of impacting dilute spray on surfaces beyond the Leidenfrost temperature, *Proceedings of the ASME National Heat Transfer Conference*, Pittsburgh, Pennsylvania, Vol. 87-HT-1, pp. 1–8 (1987).
16. E. A. Mizikar, Spray cooling investigation for continuous casting of billets and blooms, *Iron Steel Engng* **47,** 53–60 (1970).
17. K. Sasaki, Y. Sugitani and M. Kawasaki, Heat transfer in spray cooling on hot surface, *Tetsu-To-Hagane* **65,** 90–96 (1979).
18. J. K. Brimacombe, P. K. Agarwal, L. A. Baptista, S. Hibbins and B. Prabhakar, Spray cooling in the continuous casting of steel, *Proceedings of the National Open Hearth and Basic Oxygen Steel Conference*, Washington, D.C., Vol. 63, pp. 235–252 (1980).
19. L. Bolle and J. C. Moureau, Experimental study of heat transfer by spray cooling. In *Heat and Mass Transfer in Metallurgical Systems* (Edited by D. B. Spalding and N. H. Afgan), pp. 527–534. McGraw-Hill, New York (1981).
20. W. P. Klinzing, J. C. Rozzi and I. Mudawar, Film and transition boiling correlations for quenching of hot surfaces with water sprays, *J. Heat Treating* **9,** 91–103 (1992).
21. K. J. Choi and S. C. Yao, Mechanisms of film boiling heat transfer of normally impacting spray, *Int. J. Heat Mass Transfer* **30,** 311–318 (1987).
22. S. C. Yao and K. J. Choi, Heat transfer experiments of mono-dispersed vertically impacting sprays, *Int. J. Multiphase Flow* **13,** 639–648 (1987).
23. K. J. Choi and B. S. Kang, Parametric studies of droplet-wall direct heat transfer in spray cooling process, *Proceedings of the* 1993 *ASME Winter Annual Meeting*, New Orleans, Louisiana, Vol. 178/HTD-270, pp. 161–165 (1993).
24. B. Delcorio and K. J. Choi, Analysis of direct liquid-solid contact heat transfer in monodispersed spray cooling, *J. Thermophy. Heat Transfer* **5,** 613–620 (1991).
25. A. Moriyama, K. Araki, M. Yamagami and K. Mase, Local heat-transfer coefficient in spray cooling of hot surface, *Trans. Int. Steel Inst. Japan* **28,** 104–109 (1988).
26. S. Deb and S. C. Yao, Analysis of film boiling heat transfer of impacting sprays, *Int. J. Heat Mass Transfer* **32,** 2099–2122 (1989).
27. G. Brenn and A. Frohn, An experimental method for the investigation of droplet oscillations in a gaseous medium, *Exp. Fluids* **15,** 85–90 (1993).
28. R. N. Berglund and B. Y. H. Liu, Generation of monodisperse aerosol standards, *Envir. Sci. Technol.* **7,** 147–153 (1973).
29. K. Anders, N. Roth and A. Frohn, Operation characteristics of vibrating-orifice generators: the coherence length, *Particle Particle Syst. Charact.* **9,** 40–43 (1992).

30. K. Anders, N. Roth and A. Frohn, The velocity change of ethanol droplets during collision with a wall analyzed by image processing, *Exp. Fluids* **15,** 91–96 (1993).
31. L. Rayleigh, On the instability of jets, *Proc. London Math. Soc.* **10,** 4–13 (1878).
32. J. M. Schneider and C. D. Hendricks, Source of uniform-sized liquid droplets, *Rev. Scient. Instrum.* **35,** 1349–1350 (1964).
33. I. Mudawar and W. S. Valentine, Determination of the local quench curve for spray-cooled metallic surfaces, *J. Heat Treating* **7,** 107–121 (1989).
34. D. D. Hall, A method of predicting and optimizing the thermal history and resulting mechanical properties of aluminum alloy parts subjected to spray quenching, M.S. Thesis, Purdue University, West Lafayette, IN (1993).